Electronic band structure of sulphide spinels CuM_2S_4 (M=Co, Rh,Ir)

1995 J. Phys.: Condens. Matter 7 4433

(http://iopscience.iop.org/0953-8984/7/23/012)

J. Phys.: Condens. Matter 7 (1995) 4433–4445. Printed in the UK

Electronic band structure of sulphide spinels CuM_2S_4 (M = Co, Rh, Ir)

Tatsuki Oda†§, Masafumi Shirai†, Naoshi Suzuki† and Kazuko Motizuki‡

† Department of Physics, Faculty of Engineering Science, Osaka University, Machikaneyama-cho 1-3, Toyonaka 560, Japan

‡ Department of Applied Physics, Faculty of Science, Okayama University of Science, Ridai-cho 1-1, Okayama 700, Japan

Received 24 March 1995, in final form 19 April 1995

Abstract. Full-potential linearized augmented-plane-wave band calculations based on the local density approximation are performed for three sulphide spinels CuM_2S_4 (M = Co, Rh, Ir). The electronic states near the Fermi level consist mainly of the M $nd\varepsilon$ (n = 3 for Co, 4 for Rh, 5 for Ir) and the S 3p orbitals. A large $d\gamma$–$d\varepsilon$ splitting of the M nd bands is attributed mainly to the effects of hybridization between the M $nd\gamma$ and the S 3p orbitals. The Co 3d orbitals are more localized compared with the Rh 4d and the Ir 5d orbitals. Among the three compounds, the density of states or the partial density of states of the M nd components at the Fermi level is largest in $CuCo_2S_4$. The Cu 3d orbitals form relatively narrow bands. Judging from the number of Cu 3d electrons in the muffin-tin sphere the valence of the Cu ions is Cu^{1+} rather than Cu^{2+}. Hence the Cu ions are expected to be non-magnetic.

1. Introduction

Spinel compounds, AB_2X_4, show various properties according to various atomic combinations of A, B and X. In the group CuM_2S_4 (M = Co, Rh, Ir), each material shows a metallic electronic resistivity at room temperature, and different ordered phases are observed at low temperatures though the B site is occupied by an atom of the same group in the periodic table.

$CuCo_2S_4$ shows an antiferromagnetic order below the Néel temperature $T_N = 18$ K [1]. The temperature dependence of the static magnetic susceptibility χ has been measured by Miyatani and co-workers [1]. They have decomposed χ above T_N into a Curie–Weiss term and a temperature-independent term and have concluded that the effective magnetic moment, $0.89\mu_B$ per formula unit, estimated from the Curie constant is attributed to that of the Cu atom with the electronic configuration $(3d)^9$. It has also been found that the temperature-independent term of χ is greatly enhanced in comparison with that of $CuRh_2S_4$.

$CuRh_2S_4$ has been well known as a superconductor with $T_c = 4$–5 K since 1967 [2,3]. The specific heat has been measured in the superconducting state, as well as in the normal state, by Hagino and co-workers [4]. From these results, in the normal state the electronic specific heat coefficient γ has been estimated to be 25 mJ K^{-2} mol^{-1} and the Debye temperature to be 230 K. They have also obtained the normalized jump of the specific heat at the transition temperature, $\Delta C/\gamma T_c$, to be 1.82. Measurements of nuclear

§ Present address: Department of Physics, Faculty of Science, Kanazawa University, Kakuma-machi, Kanazawa 920-11, Japan.

0953-8984/95/234433+13$19.50

magnetic resonance (NMR) at Cu sites in $CuRh_2S_4$ have been carried out by Kumagai and co-workers [5]. The nuclear-spin lattice relaxation rate T_1^{-1} below T_c shows a coherence peak and exponential decay, from which the normalized gap $2\Delta_0/k_BT_c$ has been estimated to be about 3.6. These experimental results suggest that $CuRh_2S_4$ is a BCS-type superconductor.

$CuIr_2S_4$, which has been recently synthesized, shows a metal–insulator transition at $T_t \simeq 230$ K accompanying a structural phase transition [6–8]. The transition is of first order, with a volume reduction of about 0.7% just below T_t [7]. The crystal structure above T_t is the normal spinel structure and that below T_t is tetragonal with an axial ratio of about 1.03 [7]. The atomic positions below T_t have been determined by a Rietveld analysis of the x-ray diffraction pattern assuming a tetragonal structure with the space group $I4_1/amd$ [7]. However, there are some weak reflections that cannot be explained by the assumed structure. It seems to indicate the existence of further small atomic displacements that cause some superstructure.

In $CuIr_2S_4$ the magnetic susceptibility χ shows a Pauli paramagnetic behaviour above T_t and shows an almost temperature-independent diamagnetic behaviour below T_t [7, 8]. The abrupt decrease of χ at T_t has been attributed to disappearance of the Pauli paramagnetic susceptibility $\chi_P = \mu_B^2 N^\chi(E_F)$ due to the metal–insulator transition, and the density of states $N^\chi(E_F)$ at the Fermi level has been estimated to be 0.67 states eV^{-1} $atom^{-1}$ (128 states Ryd^{-1} per unit cell) [7, 8]. The activation energy in the insulating state is estimated from the temperature dependence of the electrical resistivity [6–8] and from the temperature dependence of T_1^{-1} in the NMR measurements [5]. The estimated values by the two different measurements are almost the same, and are about 0.04–0.05 eV.

Since there has been no report about the electronic structure for CuM_2S_4, we have performed full-potential linearized augmented-plane-wave (FLAPW) band calculations for these three spinels to obtain a unified understanding of their physical properties as well as to establish a basis for clarifying the mechanisms of their phase transitions. The results of the FLAPW band calculations for CuM_2S_4 are presented in section 2, and discussions focused on the phase transitions in CuM_2S_4 are given in section 3. A summary of the present study is also given in section 3.

2. Electronic structure of CuM_2S_4 (M = Co, Rh, Ir)

CuM_2S_4 has a normal spinel structure with the space group $Fd3m$ (O_h^7). The unit cell contains two formula units (14 atoms). The Cu atoms occupy the A site which is tetrahedrally surrounded by S atoms and the M atoms the B site which is octahedrally surrounded by S atoms. In table 1 we show all the atomic positions in CuM_2S_4. There is an internal structural parameter u, which determines the actual positions of the S atoms in the unit cell. In ideal spinel structure the value of u is $u_{ideal} = 3/8 = 0.375$, in which case the S atoms form a perfect face-centred cubic (FCC) lattice. In the actual structure $u_{real} \simeq u_{ideal} + 0.01$. As a result the crystal field acting on the M site has a trigonal component.

2.1. Calculational procedure

The FLAPW method is one of the most reliable procedures for electronic structure calculations in the framework of the local density approximation (LDA). In this method the space in each unit cell is divided for convenience into two regions: the muffin-tin (MT) region inside the MT spheres associated with each atom, and the interstitial region defined as the space other than the MT region. The basis functions, which are independent of the eigen-energies, are

Table 1. The atomic positions in CuM_2S_4 (taking the $\bar{3}m$ site as the origin). The internal structural parameter u, which determines the actual positions of the S atoms, is about 0.385.

Atom	Site	Atomic position (units of a)
Cu	$8a$	$(\pm\frac{1}{8}, \pm\frac{1}{8}, \pm\frac{1}{8})$
M	$16d$	$(0, 0, \frac{1}{2})$, $(0, -\frac{1}{4}, \frac{1}{4})$, $(-\frac{1}{4}, 0, -\frac{1}{4})$, $(-\frac{1}{4}, -\frac{1}{4}, \frac{1}{2})$
S	$32e$	$(\pm u, \pm u, \pm u)$, $(\frac{1}{2} \pm u, \frac{3}{4} \mp u, \frac{1}{4} \mp u)$, $(\frac{1}{4} \mp u, \frac{1}{2} \pm u, \frac{3}{4} \mp u)$, $(\frac{3}{4} \mp u, \frac{1}{4} \mp u, \frac{1}{2} \pm u)$

Equivalent positions + $(0, \frac{1}{2}, \frac{1}{2})$, $(\frac{1}{2}, 0, \frac{1}{2})$, $(\frac{1}{2}, \frac{1}{2}, 0)$.

pure plane waves in the interstitial region and in the MT region they are expanded in terms of atomic-like wavefunctions obtained by solving the radial Schrödinger equation in each MT sphere [9, 10]. In the present calculation we have used the basis functions proposed by Takeda and Kübler [10]. In the FLAPW method the potential is treated essentially with no shape approximation. Practically, the potential and also the charge density are expressed by the Fourier series in terms of plane waves in the interstitial region and by the expansion in terms of the spherical harmonic functions in each MT sphere [11].

Table 2. The lattice constants and the muffin-tin (MT) radii used in the present calculations for CuM_2S_4 (M = Co, Rh, Ir).

	a (Å)	u	MT radius (Å)		
			Cu	M	S
$CuCo_2S_4$	9.4504[a]	0.386[a]	0.98474	1.08680	1.03397
$CuRh_2S_4$	9.7849[b]	0.385[b]	0.98474	1.20163	1.03397
$CuIr_2S_4$	9.8474[c]	0.385[c]	0.98474	1.24077	1.03397

[a] From [1].
[b] From [12].
[c] From [7].

In table 2 we give the lattice constants and MT radii used in our FLAPW band calculations for CuM_2S_4. For the exchange-correlation potential a Gunnarsson–Lundqvist-type potential [13] is used. We consider electrons in $[Ar]^{18}$ states for Cu or Co, $[Kr]^{36}$ states for Rh, $[Xe]^{54}(4f)^{14}$ states for Ir and $[Ne]^{10}$ states for S as 'core' electrons, which are treated as relaxed. Relativistic effects other than the spin–orbit interaction are included (scalar relativistic treatment [14]) for both the core and valence states. The criteria adopted for constructing the basis functions are $\ell_{max} = 7$ inside the MT spheres and $|k + G|_{max} \leqslant 8.7 \times 2\pi/a$ outside the MT spheres, where k denotes a vector in the first Brillouin zone (BZ) and G a reciprocal lattice vector. The latter criterion yields a set of about 700 basis functions. The potential inside the MT spheres is expanded up to $\ell_{max} = 4$, while outside the MT spheres it is expanded in a Fourier series by using more than 5600 plane waves. During the self-consistent calculation of the potential, a linearly energy-interpolated tetrahedron scheme with the use of 44 inequivalent sampling k points is adopted for the BZ integration. The self-consistency calculation is terminated when the RMS difference between the input and output potentials becomes less than 0.1 mRyd.

2.2. Band structure, density of states and Fermi surface

The energy band dispersions for CuM_2S_4 (M = Co, Rh, Ir) are shown in figures 1(*a*)–(*c*). At first glance the energy band structures for CuM_2S_4 reveal many common features. The

valence bands of CuM_2S_4 extend over a wide energy range and their bandwidth is 0.5–0.6 Ryd. The Fermi level E_F lies near the top of the valence bands and there is one hole per formula unit. Separated by a gap from the valence bands there exist unoccupied bands with a bandwidth of about 0.15 Ryd.

The total densities of states (DOS) for $CuCo_2S_4$, $CuRh_2S_4$ and $CuIr_2S_4$ are shown in figures 2(*a*), 2(*b*) and 2(*c*), respectively, together with the partial DOS of the Cu 3d, the M *n*d ($n = 3$ for Co, 4 for Rh, 5 for Ir) and the S 3p orbitals inside each MT sphere. If we look into the details of the partial DOS, there exist a couple of distinct differences among the three spinels. As seen from figures 2(*a*)–(*c*) the width of the Co 3d bands is narrower than that of the Rh 4d or the Ir 5d bands. In other words, the Co 3d orbitals are more localized compared with the Rh 4d and the Ir 5d orbitals. Among the three spinels, the total DOS or the partial DOS of the M *n*d component at E_F is largest in $CuCo_2S_4$. The total and partial DOS at E_F for CuM_2S_4 are listed in table 3. The total DOS increases from $CuIr_2S_4$ to $CuRh_2S_4$ to $CuCo_2S_4$. In all three spinels the partial DOS of the Cu 3d component is very small at E_F, and the partial DOS of the M *n*d and the S 3p components are comparable at E_F. Therefore, in a discussion of physical properties such as the transport properties and superconductivity, in which the electronic states near E_F play important roles, the contributions from the S 3p states as well as from the M *n*d states should be taken into account.

Table 3. The density of states at the Fermi level $N(E_F)$ for CuM_2S_4 (M = Co, Rh, Ir).

	$N(E_F)$ (states Ryd^{-1} per unit cell)			
	Cu(3d)	M(*n*d)	S(3p)	Total
$CuCo_2S_4$	12	114	72	255
$CuRh_2S_4$	9	34	51	130
$CuIr_2S_4$	4	30	27	83

The partial DOS of the 3d component of Co in $CuCo_2S_4$ is 29 states Ryd^{-1} per Co atom at E_F. This value is comparable with that in the non-magnetic state of FCC Co (27 states Ryd^{-1} $atom^{-1}$ [15, 16]) which shows the ferromagnetic order. The electronic specific heat coefficient of $CuRh_2S_4$ evaluated from the relation $\gamma = \frac{1}{3}\pi^2 k_B^2 N(E_F)$ is 11 mJ K^{-2} mol^{-1}, which is about half of the experimental value [4]. The difference between theory and experiment will be attributed to the effects of the electron–phonon interaction and/or the electron correlation. From the calculated total DOS, $N(E_F)$, of $CuIr_2S_4$ and the experimental DOS, $N^X(E_F)$, estimated from the static susceptibility measurements [7, 8], the Stoner enhancement factor S defined by $S \equiv N^X(E_F)/N(E_F)$ is estimated to be 1.5, which is comparable with the Stoner enhancement factors 1.1 and 1.4 obtained theoretically for FCC Cu and FCC Ir, respectively [16].

In an oxide spinel $LiTi_2O_4$, which is a superconductor with $T_c \simeq 12$ K [17], the total DOS at E_F has been evaluated to be 3.2 states eV^{-1} per formula unit (87 states Ryd^{-1} per unit cell) [18]. This value is relatively smaller than that evaluated for $CuRh_2S_4$. The electronic states at E_F in $LiTi_2O_4$ mainly consist of the Ti 3d states (about 70%) and the contribution from the O 2p states is only about 10% [18]. This fact makes a striking contrast to the present result for CuM_2S_4, in which the M *n*d and the S 3p states contribute comparably to the electronic states at E_F.

As seen from the dispersion curves in figure 1(*c*), E_F of $CuIr_2S_4$ is crossed by two bands, which give two sheets of Fermi surfaces as depicted in figures 3(*a*) and 3(*b*). The Fermi surfaces of $CuRh_2S_4$ are quite similar to those of $CuIr_2S_4$ as supposed from the similarity

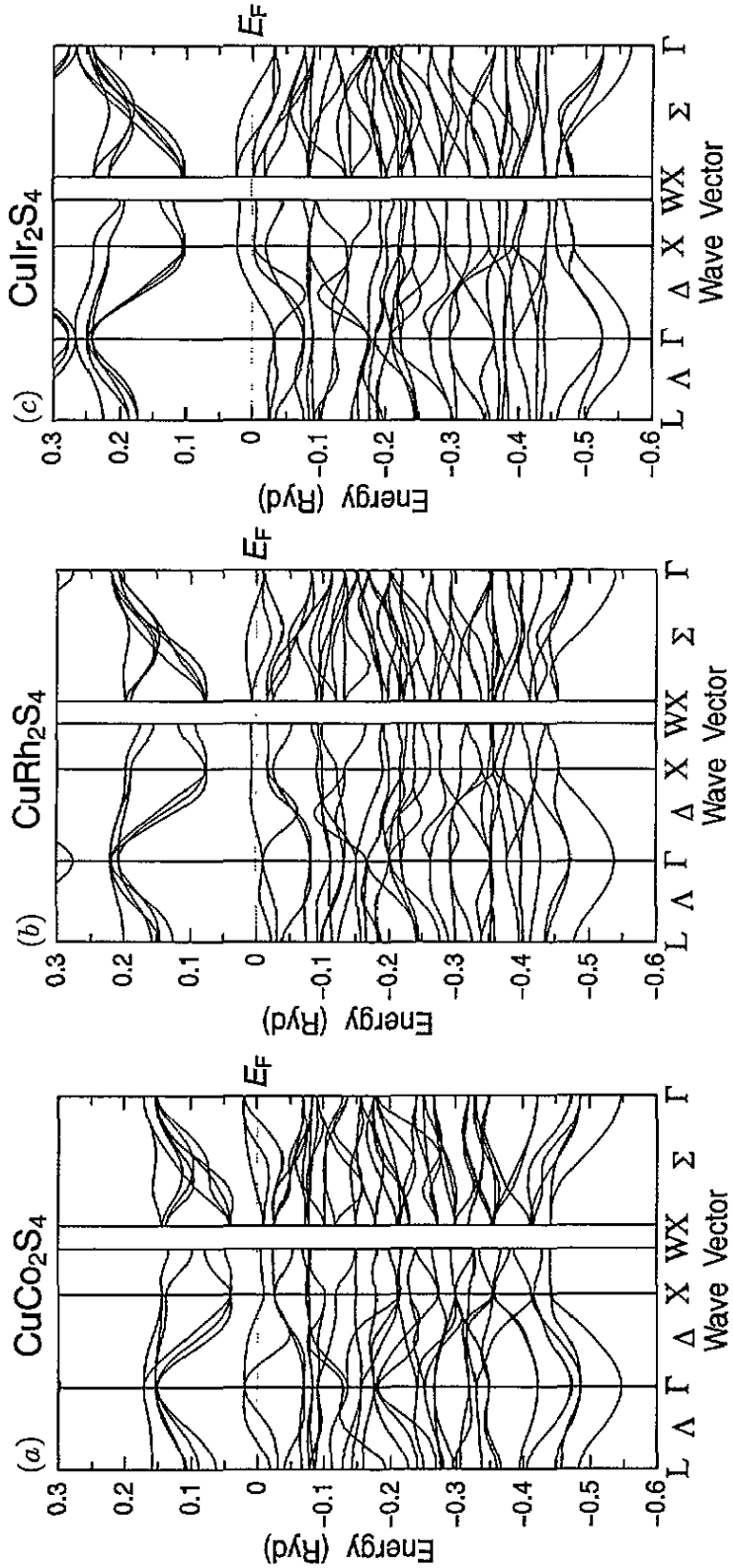

Figure 1. The energy band dispersions for (*a*) $CuCo_2S_4$, (*b*) $CuRh_2S_4$ and (*c*) $CuIr_2S_4$.

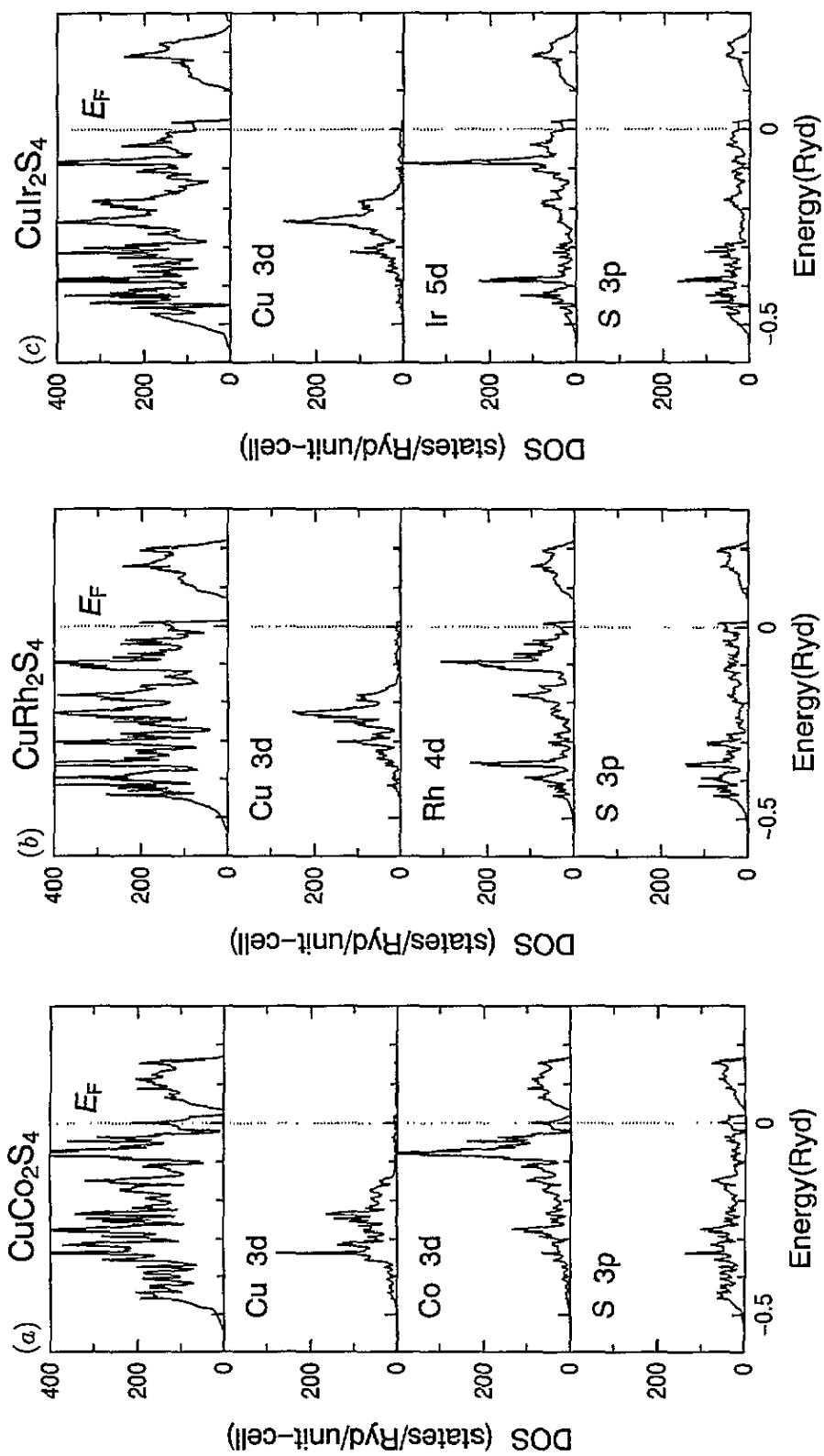

Figure 2. The total and partial densities of states of the Cu 3d, the M *nd* ($n = 3$ *for Co, 4 for Rh, 5 for Ir*) and S 3p orbitals for (*a*) $CuCo_2S_4$, (*b*) $CuRh_2S_4$ and (*c*) $CuIr_2S_4$.

in dispersion curves near E_F of both spinels (see figures 1(*b*) and 1(*c*)). From the shape of the Fermi surfaces in figures 3(*a*) and 3(*b*) we cannot expect a remarkable nesting effect of the Fermi surface as seen in La_2CuO_4 [19]. The Fermi surfaces of $CuCo_2S_4$ consist of three sheets because three bands cross E_F (see figure 1(*a*)) and their shapes are considerably different from those of $CuIr_2S_4$ or $CuRh_2S_4$. No remarkable nesting effect of Fermi surface is expected for $CuCo_2S_4$.

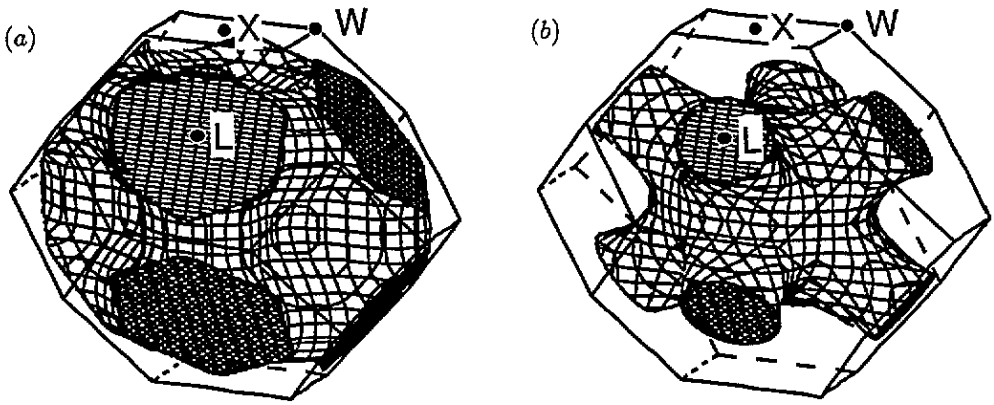

Figure 3. The Fermi surfaces of (*a*) the lower band and (*b*) the upper band for $CuIr_2S_4$.

2.3. Nature of hybridization between M nd and S 3p and between Cu 3d and S 3p

As seen from figures 2(*a*)–(*c*) the M *n*d and the S 3p orbitals hybridize strongly in a wide energy range. To see this behaviour of hybridization in more detail we have calculated the partial DOS of the $nd\varepsilon$ and $nd\gamma$ components of the M *n*d orbitals. The results for $CuCo_2S_4$ are shown in figure 4. The results for $CuRh_2S_4$ and $CuIr_2S_4$ are similar to those for $CuCo_2S_4$. The symbols, e_g^1, a_{1g} and e_g^2 in figure 4 specify the symmetrized 3d orbitals of Co: e_g^1 corresponds to the dγ orbitals, and a_{1g} and e_g^2 to the dε orbitals. The a_{1g} orbital extends along the trigonal axis and has a d$(yz + zx + xy)$-type symmetry. On the other hand, the e_g^2 orbitals extend in the plane normal to the trigonal axis and their symmetry is of d$(yz + zx - 2xy)$ or d$(yz - zx)$ type. From figures 2(*a*) and 4 we see that the Co 3dγ orbitals hybridize with the S 3*p* orbitals in the unoccupied bands (dγ–p antibonding bands) and also near the bottom of the valence bands (dγ–p bonding bands). The nature of this dγ–p hybridization seems to be dpσ bonding, judging from the octahedral coordination of the S atoms around the Co atom. Contrary to the dγ orbitals, the Co 3dε orbitals hybridize with the S 3p orbitals in the valence bands and the electronic states near E_F are mainly composed of the Co 3dε and the S 3p orbitals. The nature of the dε–p hybridization is considered to be dpπ bonding. Both $CuRh_2S_4$ and $CuIr_2S_4$ show almost the same behaviour of hybridization as that of $CuCo_2S_4$.

In order to investigate the electronic states near E_F in more detail, we have calculated the averaged charge density defined by

$$\rho(r, E_F) = e\sum_{nk}|\Psi_{nk}(r)|^2\delta(E_{nk} - E_F)\left(\sum_{nk}\delta(E_{nk} - E_F)\right)^{-1}. \qquad (1)$$

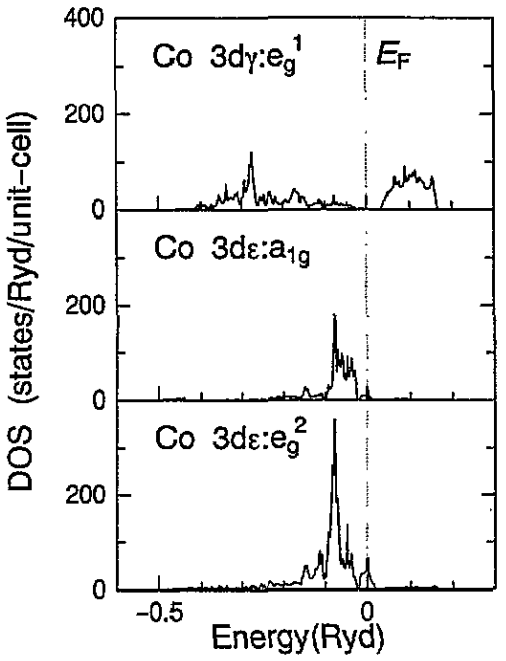

Figure 4. The partial densities of states of the Co 3d components for $CuCo_2S_4$. Here e_g^1 represents the 3dγ orbital, and a_{1g} and e_g^2 represent the 3dε orbitals which extend along the trigonal axis and in the plane normal to the trigonal axis, respectively.

The contour maps of $\rho(\boldsymbol{r}, E_F)$, calculated for $CuCo_2S_4$ in a (001) plane cutting the Co and S atoms and in a $(1\bar{1}0)$ plane cutting the Cu, Co and S atoms, are shown in figures 5(*a*) and 5(*b*), respectively. In figure 5(*a*) the d(xy) character of the Co 3dε orbitals can be seen clearly. The d($yz + zx - 2xy$) character of the Co 3dε (e_g^2) orbitals, which extend in a plane normal to the trigonal axis at each Co site, is found in figure 5(*b*). These features are consistent with the fact that the partial DOS of the e_g^2 orbitals at E_F is larger than that of the a_{1g} orbital, which extends along the respective trigonal axis. Figures 5(*a*) and 5(*b*) show the presence of the hybridization between the Co 3d and the S 3p orbitals, while the hybridization between the Cu 3d and the S 3p orbitals is hardly seen, as shown in figure 5(*b*).

As seen from figure 4 there is a gap between the Co 3dγ bands (precisely speaking, the dγ–p antibonding bands) and the Co 3dε bands in $CuCo_2S_4$. This dγ–dε splitting also exists in the Rh 4d bands in $CuRh_2S_4$ and the Ir 5d bands in $CuIr_2S_4$. We have evaluated the magnitude of the splitting $\Delta E_{d\gamma-d\varepsilon}$ by estimating the orbital energies of the M ndγ and the M ndε states in the crystal with the use of the partial DOS obtained by the present band calculation. Since there is hybridization between the M nd and the S 3p orbitals, it is rather difficult to give a strict definition of each orbital energy in the crystal. Here we have determined tentatively the orbital energies in the following way. The orbital energies of the M dε and the S 3p states are determined as the centres of gravity of the M dε and the S 3p partial DOS, respectively. On the other hand, the M dγ orbital energy is determined as the centre of gravity of the M dγ partial DOS in the dγ–p antibonding bands. The orbital energies and the dγ–dε splitting calculated in this way are listed in table 4. It is clearly seen that the magnitude of the dγ–dε splitting increases from $CuCo_2S_4$ to $CuRh_2S_4$ to $CuIr_2S_4$. The origin of this dγ–dε splitting is discussed in section 3.

Compared with the M nd orbitals the Cu 3d orbitals form rather narrow bands, as clearly seen from figures 2(*a*)–(*c*). To see the behaviour of hybridization between the Cu 3d and the S 3p orbitals we have calculated the partial DOS of the 3dε and the 3dγ components

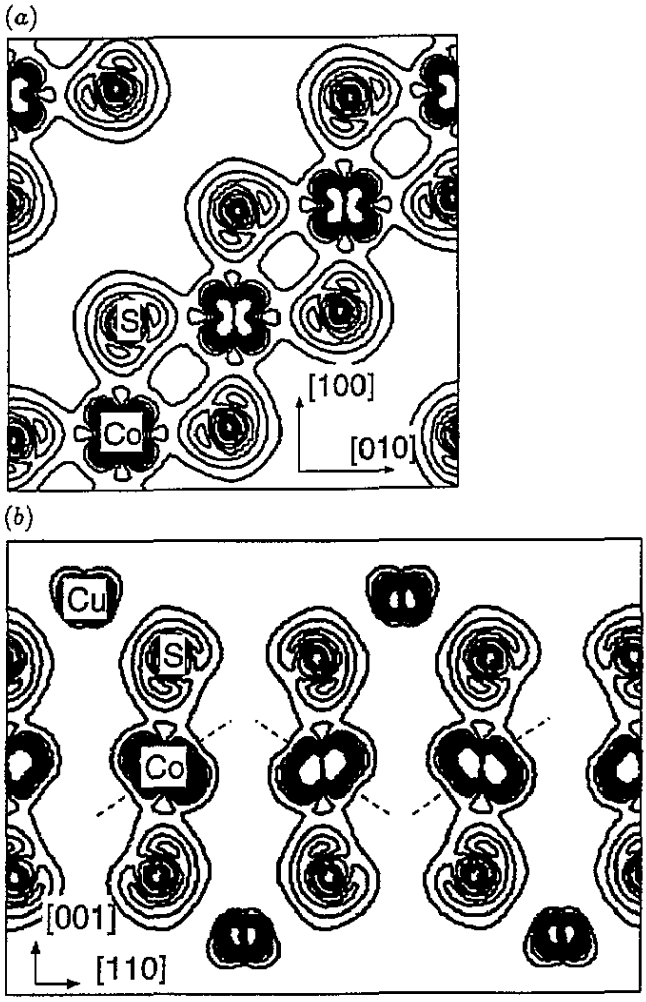

Figure 5. The contour map of the average charge density defined by (1) for $CuCo_2S_4$ (*a*) in a (001) plane cutting the Co and S atoms and (*b*) in a $(1\bar{1}0)$ plane cutting the Cu, Co and S atoms. Contours are given from 0.001 to 0.020 in steps of 0.001 e/a_B^3. Broken lines represent the trigonal axis at each Co site.

Table 4. The orbital energies of the M dγ, the M dε and the S 3p orbitals, and the dγ–dε splitting $\Delta E_{d\gamma-d\varepsilon}$ for CuM_2S_4 (M = Co, Rh, Ir).

	Orbital energy (Ryd)			$\Delta E_{d\gamma-d\varepsilon}$ (Ryd)
	M dγ	M dε	S 3p	
$CuCo_2S_4$	0.10	−0.10	−0.19	0.20
$CuRh_2S_4$	0.15	−0.14	−0.17	0.29
$CuIr_2S_4$	0.19	−0.14	−0.20	0.33

of the Cu 3d orbitals. The results for $CuCo_2S_4$ are shown in figure 6. From figures 2(*a*) and 6 we see weak hybridization between the Cu 3dε and the S 3p orbitals, while the Cu 3dγ orbitals are little hybridized with the S 3p orbitals.

The number of electrons n_ℓ for each orbital component ℓ (= 0, 1, 2, 3) in the MT sphere

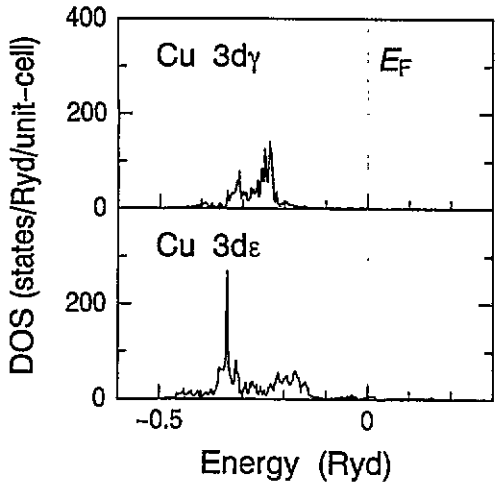

Figure 6. The partial densities of states of the 3dγ and the 3dε components of the Cu 3d orbitals in $CuCo_2S_4$.

is listed in table 5. We have obtained n_2(Cu) $\simeq$ 8.5 for all three spinels. It should be noted here that by integrating the Cu 3d partial DOS the total Cu 3d states within the MT sphere of a Cu atom are estimated to be 8.7 states per Cu atom. Therefore, n_2(Cu) $\simeq$ 8.5 means that the Cu 3d orbitals are almost completely occupied by electrons. From this result we can conclude that the valence of the Cu ions is Cu^{1+} rather than Cu^{2+}. The value of n_2 for the M atoms is larger than 6.0 in all three spinels. This is a consequence of the hybridization between the M ndγ and the S 3p orbitals. It is noted here that the value of n_2(Co) is largest, despite the fact that the MT radius of Co atoms is smallest among the three M atoms. This also indicates clearly the localized character of the Co 3d orbitals.

Table 5. The number of electrons for each orbital component ℓ (= 0, 1, 2, 3) in the muffin-tin sphere for CuM_2S_4 (M = Co, Rh, Ir).

	Orbital component ℓ				Total
	0	1	2	3	
$CuCo_2S_4$					
Cu	0.25	0.21	8.60	0.01	9.07
Co	0.28	0.32	7.07	0.02	7.69
S	1.32	2.14	0.07	0.01	3.54
$CuRh_2S_4$					
Cu	0.21	0.16	8.54	0.00	8.92
Rh	0.28	0.31	6.57	0.05	7.21
S	1.33	2.26	0.07	0.01	3.67
$CuIr_2S_4$					
Cu	0.21	0.16	8.54	0.01	8.91
Ir	0.41	0.35	6.17	0.06	7.00
S	1.32	2.28	0.09	0.01	3.70

3. Discussion and conclusion

For the origin of the dγ–dε splitting in the M nd states we can consider two kinds of effects:

one is the cubic crystal field acting on the M atoms and the other is the dpσ hybridization between M $nd\gamma$ and S 3p orbitals. In the usual crystal field theory the energy splitting of dγ and dε caused by the octahedrally coordinated ligands is given by

$$\Delta E_{d\gamma-d\varepsilon} = 10\frac{35Z|e|}{4R^5}\frac{2e}{105}\langle r^4\rangle \tag{2}$$

where $-Z|e|$ represents the effective electronic charge of the ligand atom, R is the distance between the centred atom and the ligand atoms, and $\langle r^4\rangle$ denotes the average of r^4 with respect to the radial wavefunction $R_d(r)$:

$$\langle r^4\rangle = \int |R_d(r)|^2 r^4 \cdot r^2 dr. \tag{3}$$

We have evaluated the value of $\langle r^4\rangle$ by using the radial wavefunctions inside the MT spheres which are obtained in the course of the FLAPW band calculation. The results are $\langle r^4\rangle = 0.159$, 0.366 and 0.474 Å^4 for $CuCo_2S_4$, $CuRh_2S_4$ and $CuIr_2S_4$, respectively. The values of R^5 in $CuCo_2S_4$, $CuRh_2S_4$ and $CuIr_2S_4$ are 59.4, 72.0 and 74.4 Å^5, respectively. Then, if we take $Z = 2$ tentatively, the dγ–dε splitting due to the crystal field is estimated to be $\simeq 0.02$ Ryd, which is much smaller than the values of $\Delta E_{d\gamma-d\varepsilon}$ given in table 4. This result suggests that the dγ–dε splitting in CuM_2S_4 would come mainly from the effect of dγ-p hybridization, though our estimate of the crystal field effects is not strict.

As mentioned in section 2, the results of our band calculation suggest that the electronic configuration of the Cu ions in $CuCo_2S_4$ is $(3d)^{10}$, i.e. Cu^{1+}. Then, the Cu ions will not contribute to the magnetism of $CuCo_2S_4$. On the other hand, the partial DOS of the Co 3d in the paramagnetic state of $CuCo_2S_4$ is comparable to that of FCC Co which shows the magnetic order. From these results we expect that the magnetism of $CuCo_2S_4$ would be caused by the Co atoms. This conclusion forms a striking contrast to the interpretation for the antiferromagnetism in $CuCo_2S_4$ given in [1, 20], in which the electronic configurations of the Cu and the Co ions are assumed to be Cu $(3d)^9$ and Co $(3d)^6$, respectively. In this model it is considered that the Co atoms are in the low-spin state and the magnetic moments are provided by the Cu 3d electrons.

If the on-site Coulomb interaction at Cu atoms, which may not be satisfactorily taken into account in the FLAPW calculations based on the LDA, were large enough to make an upper Hubbard band above E_F, the $(3d)^9$ electronic configuration of the Cu ions might be realized and the Cu ions would have localized magnetic moments. If so, the valence band of $CuCo_2S_4$ would be fully occupied and $CuCo_2S_4$ would be an insulator because there is an energy gap between the dγ–p antibonding band and the valence band. Experimentally, however, the electrical resistivity of $CuCo_2S_4$ shows metallic behaviour [1]. Furthermore, if the magnetic moments of $CuCo_2S_4$ were provided by the Cu atoms, we expect that the Cu ions would also have localized magnetic moments in $CuRh_2S_4$ and $CuIr_2S_4$. However, the magnetic susceptibility observed for $CuRh_2S_4$ and $CuIr_2S_4$ shows Pauli paramagnetic or diamagnetic behaviour [4, 7, 8].

According to the results of our band calculation the Cooper pairs in the superconducting state in $CuRh_2S_4$ are formed mainly by the electrons in the hybridized bands which consist of the Rh 5d and the S 3p orbitals. This situation is similar to that of $LiTi_2O_4$, in which the Cooper pairs are formed by the electrons in the hybridized bands of Ti 3d and O 2p orbitals and the lattice vibrations of the O atoms as well as those of the Ti atoms contribute to the superconductivity [18, 21–23]. Therefore, we expect that the lattice vibrations of the S atoms as well as those of the Rh atoms contribute to the superconductivity in $CuRh_2S_4$.

If we use the McMillan formula for the superconducting transition temperature T_c given by [24]

$$T_c = \frac{\Theta_D}{1.45} \exp\left(-\frac{1.04(1+\lambda_{ep})}{\lambda_{ep} - \mu^*(1+0.62\lambda_{ep})}\right) \tag{4}$$

the electron–phonon coupling constant λ_{ep} of $CuRh_2S_4$ is evaluated to be $\lambda_{ep} = 0.62$ by using the experimental values of $T_c = 4.7\,K$ and $\Theta_D = 230\,K$ (Θ_D being the Debye temperature) [4] and by assuming $\mu^* = 0.1$ (μ^* being the effective screened Coulomb repulsion constant). This value of λ_{ep} is almost the same as that of $LiTi_2O_4$ [21–23]. Therefore, the difference in T_c between $CuRh_2S_4$ and $LiTi_2O_4$ may be attributed, as pointed out by Shelton and co-workers [25], to the difference of the Debye frequency or the average frequency of the phonons contributing to the superconductivity.

Here we define λ_{tot} by

$$\gamma_{exp} = \tfrac{1}{3}\pi^2 k_B^2 N(E_F)(1+\lambda_{tot}) \tag{5}$$

where γ_{exp} represents the experimental value of the electronic specific heat coefficient and $N(E_F)$ denotes the calculated DOS at E_F. Then, by using $\gamma_{exp} = 25\,mJ\,K^{-2}\,mol^{-1}$ [4] and $N(E_F) = 130\,states\,Ryd^{-1}$ per unit cell given in table 3, the value of λ_{tot} for $CuRh_2S_4$ is estimated as 1.2. The difference $\lambda_{tot} - \lambda_{ep} \simeq 0.6$ may be attributed to the effects of the electron correlation and/or the spin fluctuations. Its value is smaller than $\lambda_{tot} - \lambda_{ep} \simeq 1.2$ of $LiTi_2O_4$ obtained in [18, 23]. This means that the effects of the electron correlation and/or the spin fluctuations are weaker in $CuRh_2S_4$ than in $LiTi_2O_4$.

The atomic displacements observed below the metal–insulator transition temperature T_t correspond to the E_g phonon mode at $q = 0$, the Γ point in the BZ, for the cubic spinel phase above T_t. We have found previously [21–23] that the electron–phonon interaction in $LiTi_2O_4$ is relatively strong for the E_g mode as well as for the A_{1g} mode. According to the results of our preliminary band calculation for $CuIr_2S_4$ with the distorted structure corresponding to the E_g mode, the electronic band structure near E_F is noticeably modified by the lattice distortion. It is thus expected that the electron–phonon interaction for the E_g mode is strong also in $CuIr_2S_4$, and that the strong electron–phonon interaction drives the structural phase transition in $CuIr_2S_4$.

As to the insulating behaviour below T_t, it is rather difficult to speculate its origin from the results of the present band calculation. In fact, our preliminary band calculation for the distorted phase of $CuIr_2S_4$ cannot predict the insulating electronic structure. Another possible origin of the insulating behaviour below T_t is the existence of some superstructure or charge-density-wave (CDW) state, which has not been confirmed by experiments so far. In x-ray diffraction measurements below T_t, weak reflections indicating the existence of some superstructure have been observed [7]. To explore a possible CDW state caused by the effect of Fermi surface nesting in $CuIr_2S_4$ we have calculated the bare electronic susceptibility defined by

$$\chi_0(q) = \sum_{nn'}\sum_{k} \frac{f(E_{n'k-q}) - f(E_{nk})}{E_{nk} - E_{n'k-q}} \tag{6}$$

where $f(E)$ is the Fermi–Dirac distribution function. As a result $\chi_0(q)$ takes a maximum value at $Q_L = (2\pi/a)(\frac{1}{2}\ \frac{1}{2}\ \frac{1}{2})$, the L point in the first BZ. Thus we can expect a possible CDW state specified by the wavevector of the L point in the first BZ. In order to present

more realistic discussion it is necessary to perform first-principles calculations of the lattice dynamics and the electron–phonon interaction in $CuIr_2S_4$, particularly for those associated with the phonons at the L point. Finally, we note that inclusion of the spin–orbit interaction might cause some change in the electronic structures of $CuIr_2S_4$ because the spin–orbit interaction becomes important, particularly in the materials including heavy elements. Thus full-relativistic band calculations including the spin–orbit interaction are desired to clarify the origin of the metal–insulator transition in $CuIr_2S_4$.

In conclusion, the main results of the present study of the electronic structure in CuM_2S_4 (M = Co, Rh, Ir) can be summarized as follows.

(i) The electronic states near E_F consist mainly of M $nd\varepsilon$ ($n = 3$ for Co, 4 for Rh, 5 for Ir) and S 3p orbitals. No remarkable Fermi surface nesting effect is found. The nature of hybridization between the M $nd\varepsilon$ and S 3p orbitals is $dp\pi$ bonding. On the other hand, the strong hybridization between the M $nd\gamma$ and S 3p orbitals is caused by $dp\sigma$ bonding, and the $d\gamma$–p bonding and antibonding bands are formed. The total DOS at E_F increases from $CuIr_2S_4$ to $CuRh_2S_4$ to $CuCo_2S_4$. In all three materials the Cu 3d component at E_F is very small, and the components of the M nd and the S 3p orbitals are comparable at E_F. A large splitting between the M $nd\gamma$ and the M $nd\varepsilon$ bands is attributed mainly to the effect of $d\gamma$–p hybridization due to strong $dp\sigma$ bonding.

(ii) The Cu 3d orbitals form relatively narrow bands. Judging from the number of Cu 3d electrons in the MT sphere, the Cu ions are expected to exist as Cu^{1+} rather than Cu^{2+}, i.e. the Cu ions in CuM_2S_4 would not have magnetic moments. The Co 3d component at E_F in $CuCo_2S_4$ is 29 states Ryd^{-1} per Co atom, which may be large enough to cause the magnetic instability in $CuCo_2S_4$. As a result, the antiferromagnetism of $CuCo_2S_4$ is expected to arise from the Co atoms.

Acknowledgments

We would like to thank Professor S Nagata of the Muroran Institute of Technology for useful discussions, and for showing us his experimental data prior to publication. Thanks are also due to Professor A Yanase and Dr H Harima of the University of Osaka Prefecture for providing us with their FLAPW program. This work is supported by Grant-in-Aid from the Ministry of Education, Science and Culture, Japan.

References

[1] Miyatani K, Tanaka T, Sakita S, Ishikawa M and Shirakawa N 1993 *Japan. J. Appl. Phys.* **32** 448
[2] Van Maaren N H, Schaeffer G M and Lotering F K 1967 *Phys. Lett.* **25A** 238
[3] Robbins M, Willens R H and Miller R C 1967 *Solid State Commun.* 5 933
[4] Hagino T, Seki Y, Wada N, Tsuji S, Shirane T, Kumagai K and Nagata S 1995 *Phys. Rev.* B to be published
[5] Kumagai K, Tsuji S, Hagino T and Nagata S 1995 *Proc. Taniguchi Conf.* to be published
[6] Nagata S, Hagino T, Seki Y and Bitoh T 1994 *Physica* B **194–6** 1077
[7] Furubayashi T, Matsumoto T, Hagino T and Nagata S 1994 *J. Phys. Soc. Japan* **63** 3333
[8] Hagino T, Tojo T, Atake T and Nagata S 1995 *Phil. Mag.* B to be published
[9] Andersen O K 1975 *Phys. Rev.* B **12** 3060
[10] Takeda T and Kübler J 1979 *J. Phys. F: Met. Phys.* **9** 661
[11] Weinert M 1981 *J. Math. Phys.* **22** 2433
[12] Furubayashi T private communications
[13] Gunnarsson O and Lundqvist B I 1976 *Phys. Rev.* B **13** 4274
[14] Koelling D D and Harmon B N 1977 *J. Phys. C: Solid State Phys.* **10** 3107

[15] Moruzzi V L, Janak J F and Williams A R 1978 *Calculated Electronic Properties of Metals* (New York: Pergamon)
[16] Sigalas M M and Papaconstantopoulos D A 1994 *Phys. Rev.* B **50** 7255
[17] Johnston D C 1976 *J. Low Temp. Phys.* **25** 145
[18] Massidda S, Yu J and Freeman A J 1988 *Phys. Rev.* B **38** 11352
[19] Pickett W E 1989 *Rev. Mod. Phys.* **61** 433
[20] Furukawa Y, Wada S, Miyatani K, Tanaka T, Fukugauchi M and Ishikawa M 1995 *Phys. Rev.* B to be published
[21] Oda T, Shirai M, Suzuki N and Motizuki K 1994 *J. Supercond.* **7** 555
[22] Oda T, Shirai M, Suzuki N and Motizuki K 1994 *J. Phys.: Condens. Matter* **6** 6997
[23] Oda T 1995 *PhD Thesis* (Osaka University)
[24] McMillan W L 1968 *Phys. Rev.* **167** 331
[25] Shelton N R, Johnston D C and Adrian H 1976 *Solid State Commun.* **20** 1077